Homogenization of unsaturated bentonite during hydration

Antonio Gens[1*], *Ramon* Vasconcelos[1], *Carlos E.* Rodríguez[2], *Jean* Vaunat[1], *María Victoria* Villar[3]

[1]Universitat Politècnica de Cataunya - CIMNE, C. Jordi Girona, 1-3, 08034 Barcelona, Spain
[2]Universitat Politècnica de Cataunya, C. Jordi Girona, 1-3, 08034 Barcelona, Spain
[3]CIEMAT, Avd. Complutense, 40, 28040 Madrid, Spain

Abstract. Bentonite barriers are a key component in may designs of deep geological repositories for high level nuclear waste. During the hydration stage, the bentonite undergoes non-uniform changes in dry density that may persist even after reaching a fully saturated state. Since dry density controls the properties of the bentonite that ensure the functions of safety of the barrier, the potential of bentonite for homogenization or otherwise is a matter of high relevance. The paper presents the results and the analyses of two hydration tests on initially heterogenous samples, especially designed to explore the phenomena and processes underlying the homogenisation of bentonite materials. The formulation and constitutive model used in the analyses are briefly presented followed by a description of the tests. Subsequently, the experimental data obtained from the tests are discussed together with the results of the hydromechanical analyses performed. Particular attention is given to the degree of homogenization of the specimens achieved at the end of the tests. The simulations have resulted in a very satisfactory agreement with test observations, especially regarding the final state of the samples, thus enhancing the confidence in the numerical tool employed.

1 Introduction

Many designs for deep geological repositories for spent fuel and high-level nuclear waste include a barrier of compacted bentonite as part of a multi-barrier system intended to delay and minimize the transport of radionuclides to the biosphere. The barrier should have a low hydraulic conductivity to ensure that advection flow is negligible compared to diffusion, and a sufficient swelling potential to seal potential voids generated during installation or subsequently (e.g. by erosion). Both properties, hydraulic conductivity and swelling potential depend strongly on the dry density (or porosity) of the material.

The bentonite of the barrier is installed in an unsaturated state and undergoes hydration by the host rock water until becoming saturated. During this transient period, the bentonite undergoes non-uniform changes in dry density that may remain even after achieving a fully saturated state. This has been observed, for instance, in the final dismantling of the Febex test where a clearly non-uniform dry density distribution was encountered at the end of the experiment in spite of the fact that the bentonite barrier was practically saturated at that stage [1,2]. The potential of the bentonite for homogenization or otherwise is therefore a matter of high relevance and has been given recently a substantial amount of attention [3]. Although temperature effects will also influence bentonite homogenization, for simplicity, thermal effects are not considered at this stage.

In this context, a series of laboratory hydration tests have been performed at the CIEMAT laboratory on samples of bentonite composed of a pellets part and a compacted block part. A proper understanding of both the processes occurring during the test and the final state of the specimen requires the performance of numerical analyses that incorporate a coupled hydromechanical formulation and an appropriate constitutive law for the material. A double structure constitutive model has been adopted in order to take into account, in an approximate manner, the microstructural features of the bentonite and their evolution.

In this paper, the formulation and constitutive model are briefly presented first, followed by a summary description of the tests. Afterwards, the experimental observations of the tests are discussed in the light of the information provided by the numerical analyses. Particular attention is given to the degree of homogenization of the specimens achieved at the end of the tests.

2 Coupled formulation and constitutive model

2.1 General

The formulation used has been developed within the conceptual framework of a double structure (or double porosity) material where two porosity levels are

* Corresponding author: antonio.gens@upc.edu

distinguished: macroporosity and microporosity [4-11]. This additional complexity is demanded by the actual microstructure of compacted bentonite where the two structural levels can be readily distinguished (Figure 1a). The microstructure corresponds to the inside of the clay aggregates whereas the macrostructure refers to the granular-like arrangement of the aggregates themselves. This distinction is even more evident if pellets-based materials are considered (Figure 1b). For brevity, only a brief summary of the formulation and constitutive equations is presented herein.

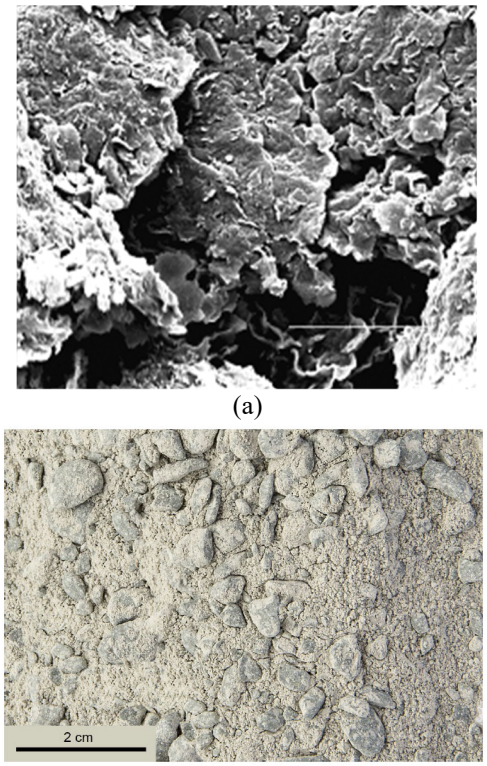

(a)

(b)

Fig. 1. a) SEM image of compacted bentonite, b) pellets-based bentonite material.

2.2 Hydromechanical formulation

Figure 2 presents a phase diagram for an unsaturated double-structure porous medium. The formulation is based on the establishment of a series of balance equations that express basic physical principles such as the conservation of mass, energy or momentum that have to be satisfied at all times and at every point of the calculation domain.

In this case, it is assumed that the two structural levels may not be in equilibrium so that water will be exchanged between them until equilibrium is established. It is further assumed that advective liquid flow only occurs in the macroporosity. Then, the relevant balance equations are:

Solid balance equation

$$\frac{D\bar{\Phi}}{Dt} = \frac{(1-\bar{\Phi}_m-\bar{\Phi}_M)}{\rho_s}\frac{D\rho_s}{Dt} + (1-\bar{\Phi}_m-\bar{\Phi}_M)\frac{d\varepsilon_v^{m\to M}}{dt} - \frac{D\bar{\Phi}_m}{Dt} \quad (1)$$

Water in macrostructure balance equation

$$\frac{D\left(\theta_{lM}^{w}S_{lM}+\theta_{gM}^{w}S_{gM}\right)}{Dt}\bar{\phi}_M + \left(\theta_{lM}^{w}S_{lM}+\theta_{gM}^{w}S_{gM}\right)\frac{d\varepsilon_{vM}}{dt} + \nabla\left(j_{lM}^{W}+j_{gM}^{W}\right) = -\Gamma^{w} \quad (2)$$

Water in microstructure balance equation

$$\frac{D\left(\theta_{lm}^{w}S_{lm}+\theta_{gm}^{w}S_{gm}\right)}{Dt}\bar{\phi}_m + \left(\theta_{lm}^{w}S_{lm}+\theta_{gm}^{w}S_{gm}\right)\frac{d\varepsilon_{vm}}{dt} + \nabla\left(j_{lm}^{W}+j_{lm}^{W}\right) = \Gamma^{w} - \left(\theta_{lm}^{w}S_{lm}+\theta_{gm}^{w}S_{gm}\right)(1-\phi)\frac{d\rho_s}{\rho_s} \quad (3)$$

Momentum balance equation

$$\nabla\boldsymbol{\sigma} + \boldsymbol{b} = 0 \quad (4)$$

where $\bar{\phi}$ is volumetric fraction, ϕ total porosity, ρ solid density, ε_v volumetric strain, θ mass fraction, S degree of saturation, $\boldsymbol{j}$ advective fluxes, Γ^{w} the water exchange term, $\boldsymbol{\sigma}$ total stress and $\boldsymbol{b}$ mass forces. Subscripts *p, m, M, s, l* and *g* mean pore, micro, macro, solid, liquid and gas, respectively, whereas superscript w refers to water.

In fact, the solid mass balance equation can be subsumed, using material derivatives, into equation (2). Also, the microstructural water balance can be solved at a local level with microstructural suction treated as a state variable. Therefore, only the balance equations for macrostructural water and momentum have to be solved at a global level in order to get the basic unknowns of liquid pressure and displacements.

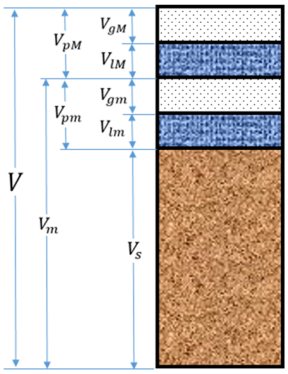

Fig. 2. Phase diagram of a double-structure unsaturated medium. *V* is volume and subscripts *p, m, M, s, l* and *g* mean pore, micro, macro, solid, liquid and gas, respectively.

2.3 Constitutive equations

The classical BBM model [12] is used for the macrostructural constitutive equation whereas the microstructural mechanical behaviour is described by the following nonlinear elastic relationship:

$$K_m = \frac{p'_m}{(1+\phi_m)\kappa_m} \quad (5)$$

where K_m is the microstructural bulk modulus, p'_m the effective mean stress acting on the microstructure and κ_m a model parameter. While net stresses and macrostructural suction control the macrostructure behaviour, mean Bishop's stress and microstructural suction define the behaviour of the microstructure. Two interaction functions (one for drying and one for wetting) [4] describe the effect of the microstructure on

the macrostructure. A full description of the mechanical constitutive model is given in [13].

Regarding the hydraulic component of the formulation, it is assumed that Darcy's law governs the advective flow of liquid. Hydraulic conductivity is strongly dependent on degree of saturation via an appropriate function for relative permeability. As the liquid advective flow occurs only in the macroporosity, intrinsic permeability does not depend on total porosity but only on the macrostructural one. The water exchange between the macro and micro-porosity is assumed proportional to the difference between micro and macro suctions. Finally, Van Genuchten expressions [14] are used for the retention curves for the macro and micro retention curves.

3 Description of the tests

The tests were carried out in the CIEMAT laboratory in Madrid using a large oedometer that allows keeping the volume constant while measuring the axial load. The specimens were 10 cm long with a diameter of 10 cm. They are divided in two halves; the lower 5 cm is occupied by bentonite pellets whereas, in the upper 5 cm, there is a compacted block of bentonite. Hydration is performed through the base porous sinter. Figure 3 shows a schematic view of the apparatus and Figure 4 the two types of material used in the tests.

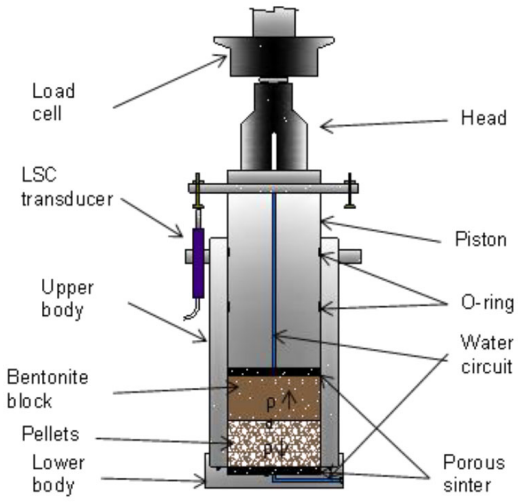

Fig. 3. Schematic view of the apparatus [15]

Febex bentonite, a calcium-magnesium-sodium bentonite, was used to form the specimens. The block was compacted with a water content of 14% to a dry density of 1.6 g/cm^3. The density of the individual pellets was 2.12 g/cm^3 but the resulting granular assembly had a dry density of 1.29 g/cm^3, much lower than that of the block.

The analysis of two tests are presented in this paper: MGR22 and MGR 23. The main difference is that in test MGR22 hydration is performed by applying a constant flow of 0.05 cm^3/h whereas in test MGR23 a constant 15 kPa pressure is applied. Also, the water content of the pellets is 10% in MGR22 and 3.5% in MGR23, Additional details of the test are provided in [15].

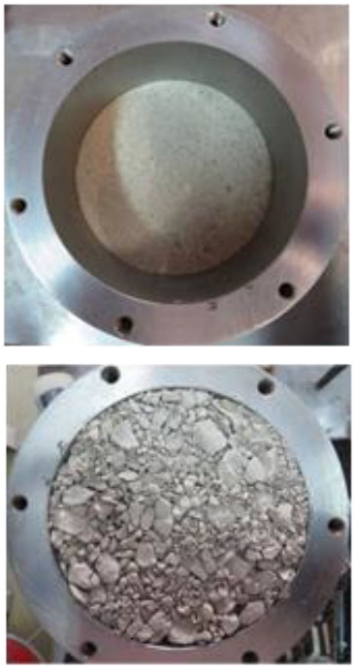

Fig. 4. Compacted bentonite block (top) and bentonite pellets (bottom)

4 Analysis of the tests and discussion

4.1 Features of the analysis

The tests have been simulated using the coupled hydromechanical formulation outlined above. The domain of analysis is axisymmetric with the same dimensions as the samples and discretised by means of 400 linear quadrangles (Figure 5). A selected integration scheme has been used to ensure a good performance of the linear elements. The parameters for the analyses have been derived from the extensive literature on the Febex bentonite available [e.g. 16-20].

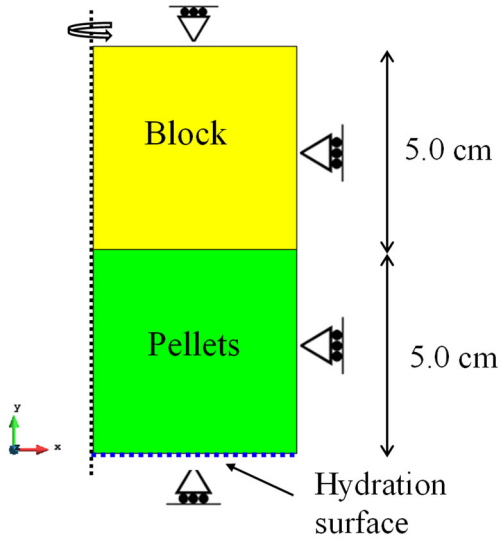

Fig. 5. Analysis domain and boundary conditions

Because of using a double structure model, micro and macro retention curves have to be defined for pellets

and blocks (Figure 6). It is also is necessary to partition the total porosity into micro and macroporosity. This has been based on the Mercury Intrusion Porosimetry (MIP) observations reported in [15]. For the block, initial porosity is 0.404, divided in 0.216 and 0.188 for the micro and macro volumetric fractions, respectively. For the pellets, initial porosity is 0.528 distributed in volumetric fractions of 0.323 (micro) and 0.205 (macro). Initial suctions are derived from the corresponding retention curves. It is assumed that, initially, micro and macro porosity are in hydraulic equilibrium.

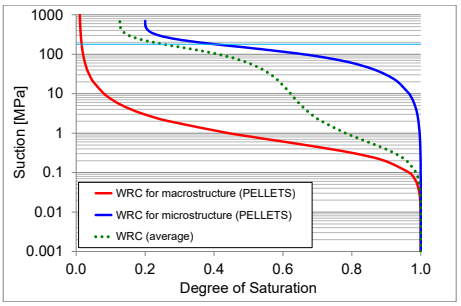

(a)

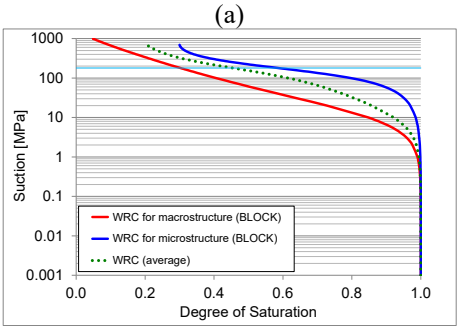

(b)

Fig. 6. Retention curves. a) Pellets, b) Block

4.2 Analysis of test MGR22 (constant flow)

The actual test protocol has been followed in the analysis. Thus, there is an initial period of 10 days without water entry followed by a water injection at a constant rate of 0.05 cm^3/h. The evolution of the computed axial stress is plotted in Figure 7, together with experimental data. It can be observed that the final swelling pressure is correctly captured. The variation of axial stress with time is also reasonably reproduced although the computed initial rate of pressure increase is faster than observed, suggesting that the water exchange parameter should be lower to delay the transfer of water from the macroporosity to the microporosity.

The progress of hydration can be observed plotting the computed evolution of porosity for three different points, one in the block and two in the pellets (Figure 8). It can be observed that the porosity in the pellets reduce while that of the block increases, the analysis suggesting that the initial difference has reduced very significantly at the end of the test.

Direct observation of the homogenization achieved is obtained from the measurements of dry density and water content at different locations at the end of the test. For test MGR22, Figures 9 and 10 show the final observed and computed distributions. It can be noted that a high degree of homogenization has been achieved, especially considering the large initial differences in dry densities. It is also noteworthy that the results of the numerical simulation are very close to the experimental data. As the sample is practically fully saturated at the end of the test, the distribution of water content follows the same pattern as that of the dry density.

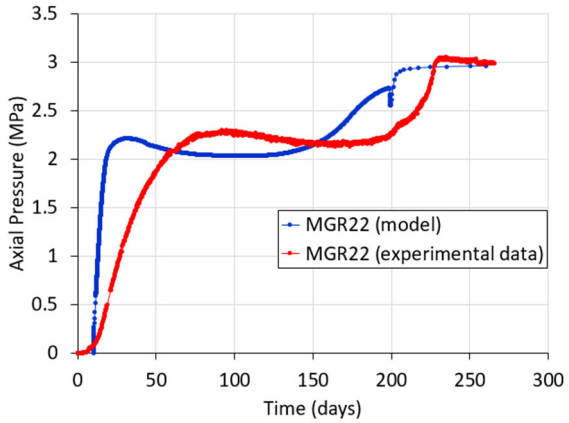

Fig. 7. Computed and observed evolution of axial stress. Test MGR 22.

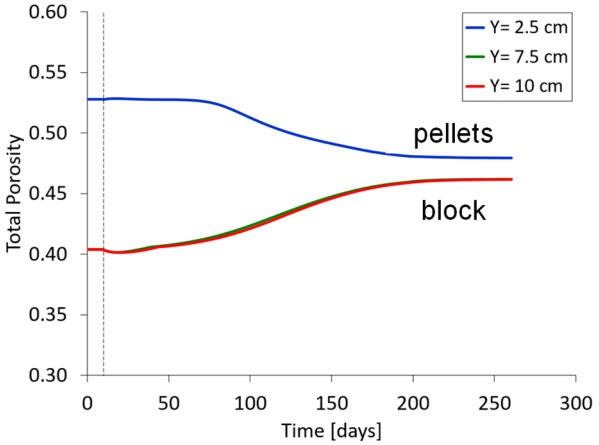

Fig. 8. Computed evolution of pellets and block porosity. Test MGR22. Y is the distance to the hydration boundary.

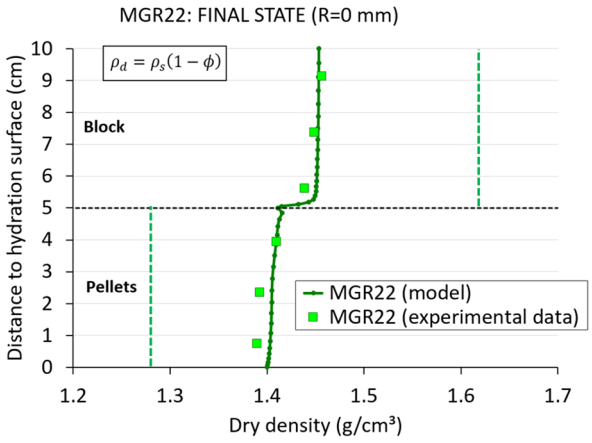

Fig. 9. Comparison of simulation results with experimental observations for the distribution of dry density at the end of test MGR22 (the vertical dashed lines indicate initial conditions).

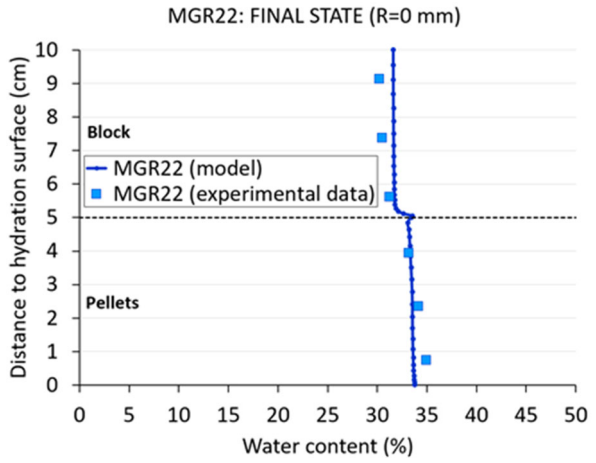

Fig. 10. Comparison of simulation results with experimental observations for the distribution of water content at the end of test MGR22.

4.3 Analysis of test MGR23 (constant pressure)

For the simulation of this test, a constant 15 kPa pressure has been applied at the hydration surface. The evolutions of the computed water intake and axial stress are plotted in Figures 11 and 12, respectively, together with experimental data. It can be noted that the initial rate of hydration is underestimated while the simulation overestimates the rate of swelling pressure increase. Those differences suggest again that the water exchange parameter should be lower. Nevertheless, the final swelling pressure is correctly reproduced.

The variations of porosity with time at the three selected points (Figure 13) show a degree of homogenization similar to that of test MGR22 in spite of their quite different hydration conditions. It appears, however, that homogenization occurs earlier in test MGR 23.

The computed and observed distribution of dry density at the ed of the test is shown in Figure 14. Again, it can be observed that a large degree of homogenization has taken place. Also, the analysis provides results very close to the observations. As the sample was also practically fully saturated at the end of the test, the distribution of water content follows the same trend as that of the dry density (Figure 15).

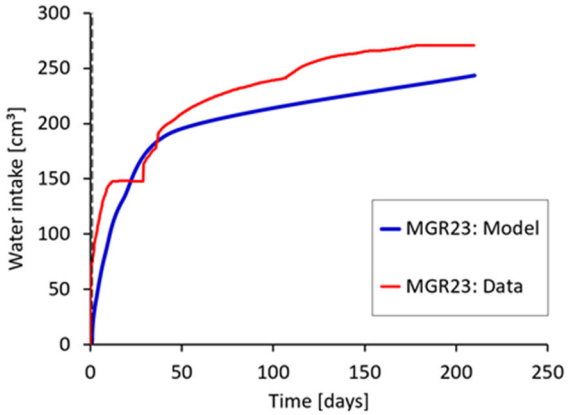

Fig. 11. Computed and observed evolution of water intake. Test MGR23

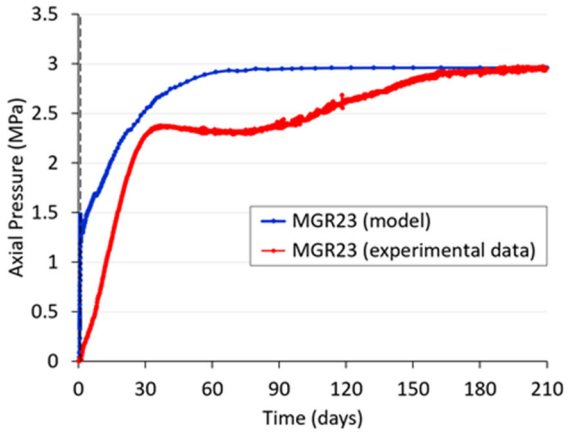

Fig. 12. Computed and observed evolution of axial stress. Test MGR23.

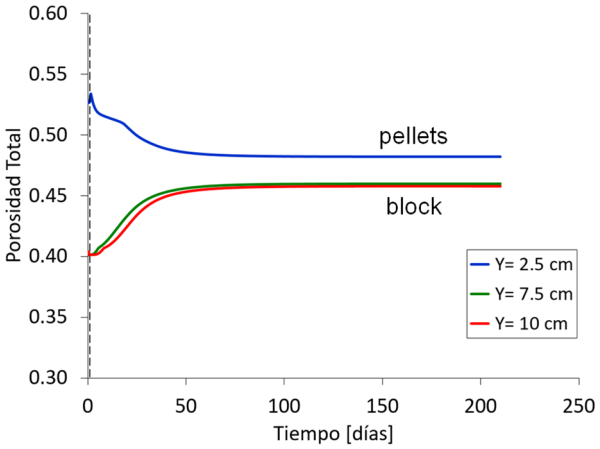

Fig. 13. Computed evolution of pellets and block porosity. Test MGR23. Y is the distance to the hydration boundary.

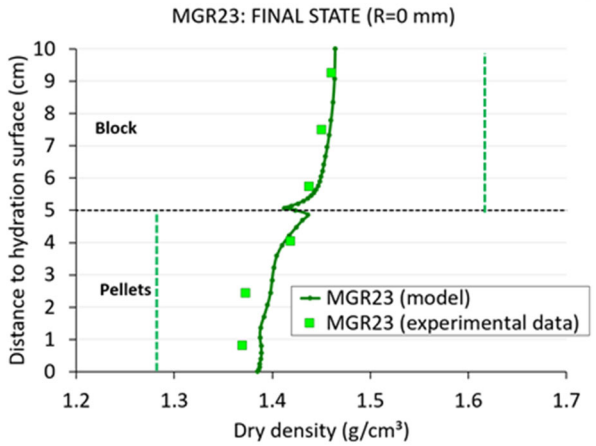

Fig. 14. Comparison of simulation results with experimental observations for the distribution of dry density at the end of test MGR23 (the vertical dashed lines indicate initial conditions).

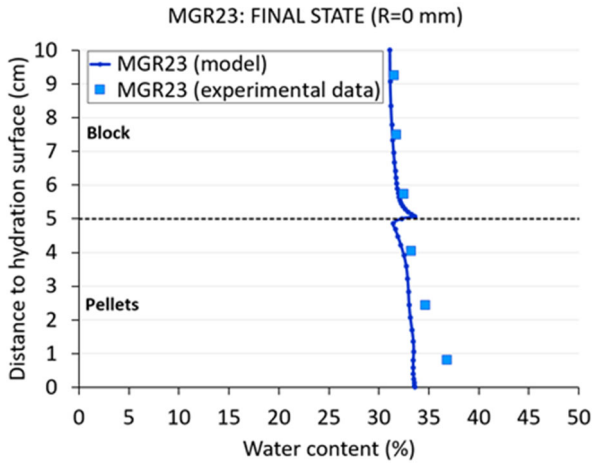

Fig. 15. Comparison of simulation results with experimental observations for the distribution of water content at the end of test MGR23.

5 Conclusions

The paper has introduced a coupled hydromechanical formulation developed in the framework of double structure materials to examine the issues of heterogeneity and homogenization during the hydration of bentonite barriers for high level nuclear waste disposal. As the performance of the barrier is critically dependent on the values of dry density, understanding of these issues is key to ensure an adequate performance of the barrier.

The formulation has been applied to the analysis of two tests especially designed to explore directly the phenomena and processes underlying the homogenisation or otherwise of heterogenous bentonite systems. The experimental results show that, for the test conditions employed, a high degree of homogenization is achieved on saturation.

The simulations have resulted in very satisfactory agreement with test observations, especially regarding the final state of the samples. Thus, it enhances confidence that the same formulation and constitutive laws can be used for predicting the evolution of heterogeneity and homogenization in other relevant settings.

Because of the use of a double structure model, the analyses provide additional information about the interplay between micro and macroporosity during the tests that has not been discussed in this paper because of space limitations.

The work presented has been developed in the framework of the Bentonite Mechanical Evolution Project (BEACON). The project receives funding from the Euratom research and training programme 2014-2018 under grant agreement No 745942. The support of Conacyt (Id. no. 710153) to the third author is also gratefully acknowledged.

References

1. M.V. Villar, R.J. Iglesias, J.L. García-Siñeriz. Environmental Geotechnics 7(2), 147–159 (2020)
2. M. Sanchez, B. Pomaro, A. Gens. Géotechnique (ahead of print) doi.org/10.1680/jgeot.21.00106. (2022).
3. P. Sellin, M. Westermark, O. Leupin, S. Norris, A. Gens, K. Wieczorek, J. Talandier, J. Swahn. EPJ Nuclear Sci. Technol. **6**, 23 (2020)
4. A. Gens, E.E. Alonso. Canadian Geotechnical Journal, **29**, 1013–32 (1992).
5. M. Sánchez, A. Gens, L do N. Guimarães, S. Olivella. Int. J. for Numerical and Analytical Methods in Geomechanics, **29**, 751–87 (2005)
6. A. Gens, A. Geotechnique, **60**, 3–74 (2010)
7. D. Mašín. Engineering Geol., **165**, 73-88 (2013)
8. A.-C. Dieudonné, G. Della Vecchia, R. Charlier. Can. Geotechnical Journal, **54**, 915-925 (2017)
9. G.M. Ghiadistri, D.M., L. Zdravković, A. Tsiampousi. *A new double structure model for expansive clays*. In: Proceedings of the 7th Int. Conf. on Unsaturated Soils, Hong Kong (2018)
10. V. Navarro, L. Asensio, H. Gharbiehb, De la Morena, J. Alonso, V.-M. Pulkkanen. Engineering Geology, **265**, 105311 (2020)
11. V. Navarro, L. Asensio, G. De la Morena, H.. Gharbiehb, J. Alonso, V.-M. Pulkkanen, V. Engineering Geology, **274**, 105714 (2020)
12. E.E. Alonso, A. Gens, A. Josa, A. Géotechnique, **40**, 405–430 (1990)
13. R.B. de Vasconcelos. *A double-porosity formulation for the THM behaviour of bentonite-based materials.* Ph.D. Thesis, Universitat Politecnica de Catalunya. (2021).
14. R. van Genuchten, R.. Water Resour. Res., **37**, 21–28 (1978)
15. M.V. Villar, R.J. Iglesias, C. Gutiérrez-Alvarez, B. Carbonell. Eng. Geology. **292**, 06272 (2021)
16. M.V. Villar, *Thermo-hydro-mechanical characterization of a bentonite from Cabo de Gata.* ENRESA Technical Publication 01/2002, Madrid. (2002).
17. A. Lloret, M.V. Villar, M.V. Physics and Chemistry of the Earth, **32**, 701-715 (2007)
18. A. Lloret, M.V. Villar, M. Sánchez, M., A. Gens, X. Pintado, E.E. Alonso. Géotechnique, **53**, 27–40 (2003)
19. A. Lloret, E. Romero, M.V. Villar, M.V. *FEBEX II Project Final report on thermo-hydro-mechanical laboratory tests*. Publicación Técnica ENRESA 10/04.Madrid. (2004)
20. C. Hoffmann, E.E. Alonso, E. Romero. Physics and Chemistry of the Earth, **32**, 832-849 (2007)